Geophysical Prospecting, 1999, 47, 551–564

Inversion of band-limited TEM responses[1]

Flemming Effersø,[2] Esben Auken[2] and Kurt Ingvard Sørensen[2]

Abstract

It is shown that the electromagnetic (EM) spectrum is characterized by strong amplitude-modulated transmitters operating in the target bandwidth of transient electromagnetic (TEM) measurements. As these transmitters cause significant noise in TEM soundings, it is mandatory to band-limit the input signals to improve the signal-to-noise ratio and thereby the depth of exploration. Band-limitation will distort the TEM responses, which leads to erroneous inversion results if the applied low-pass filters are not accounted for in the inversion scheme. We incorporate the low-pass filters in the inversion scheme and test the inversion approach on theoretical and field data. Inversion of band-limited theoretical responses results in recovery of erroneous resistivity models if the filters are not included in the inversion scheme. By contrast, inversion of band-limited theoretical and field data, for which the applied low-pass filters are included in the inversion scheme, leads to recovery of similar resistivity models, independent of the applied cut-off frequencies.

Introduction

The transient electromagnetic (TEM) method has been used extensively in Denmark over the last decade. Large TEM surveys are carried out for delineating the low-resistivity, impermeable boundaries of regional aquifers in sedimentary areas (Auken *et al.* 1994; Christensen and Sørensen 1994; Sørensen 1996). Delineation plays a major role in the long-term planning of water supply and assists in planning remediation measures to improve contaminated ground water resources.

In the literature there are several papers on noise rejection for TEM systems (e.g. Macnae, Lamontagne and West 1984; McCracken, Oristaglio and Hohmann 1986). The emphasis in these papers is on rejection of incoherent noise basically arising from lightning discharges and phase-coherent power-line noise. However, both theoretical and experimental studies suggest that amplitude-modulated (AM) long wave and very low frequency (VLF) transmitters cause high-amplitude input signals in TEM receivers that are not sufficiently band-limited. When the AM transmitter noise is sampled on logarithmically spaced gates and subsequently stacked, the standard deviation of the input signal will exhibit a t^{-1} proportionality, compared with a $t^{-1/2}$ dependence (Munkholm and Auken 1996) for white noise. The level of the AM

[1] Received April 1998, revision accepted December 1998.
[2] Department of Earth Sciences, Aarhus University, Finlandsgade 6, 8200 Aarhus N, Denmark.

transmitter noise is often orders of magnitude higher than the background noise level so that the signal-to-noise (S/N) ratio is lowered at the early and medium decay times.

Low-pass (LP) filters are used in most commercial TEM receivers to suppress the AM transmitter noise. However, the LP filters distort the early and medium part of the decay curve due to damping of the high-frequency content. The level of distortion depends on several factors such as cut-off frequency and subsurface resistivities. Thus, LP filters must be incorporated in the inversion scheme such that the calculated forward response is subject to the same filtering as the measured response.

Firstly, we characterize the EM noise spectrum based on numerical simulations and on measured noise. Secondly, we quantify the distortion of responses due to band-limitation for a number of typical resistivity models. The band-limitations are based on cut-off frequencies typically used in commercial instruments. Finally, it is demonstrated that distortion due to band-limitation can be modelled in the inversion scheme by including the LP filters in the forward response. This approach is tested on theoretical data as well as on field data.

The EM noise spectrum

EM noise can be divided into two major types, namely that arising from (i) natural sources and (ii) cultural sources. The noise spectrum has diurnal, annual and geographical variations. In the following a brief review of the sources is given. A more thorough discussion of the EM noise spectrum has been given by Macnae *et al.* (1984), McCracken *et al.* (1986) and Spies and Frischknecht (1991).

For natural sources the EM noise below 1 Hz arises mainly from complex interactions between the solar wind and the Earth's stationary magnetic field. Of more interest in TEM soundings is the spectrum above 1 Hz. The major contributor above 1 Hz is lightning discharge from thunderstorms. Distant thunderstorm activity produces a background noise level, whereas strong sferics arise from nearby or intermediate distances. These fields travel in the Earth–ionosphere cavity. Sferics occur worldwide with a frequency of ≈ 100 per second.

In populated areas cultural sources increase the overall noise level. In these areas the power distribution grid is one of the main noise contributors, resulting in spectral peaks at 50/60 Hz and associated odd harmonics. Although the voltage waveform is kept sinusoidal at 50/60 Hz, the current producing the perturbing fields fluctuates from the sinusoidal waveform due to the varying load on the grid. High-amplitude, broadband transients also occur occasionally. Furthermore, spectral peaks arising from AM transmitters around the globe contribute significant noise. These amplitude-modulated signals are transmitted with high power, such that the signals appear as distinct spectral lines, orders of magnitude higher than the ambient EM noise. The electromagnetic field from radio waves is plane-polarized and can be treated as a plane wave a few skin depths away from the transmitter antenna. The major noise contribution stems from the magnetic field, as the noise contribution from the electrical field is negligible if the receiver coil is adequately shielded.

Suppression of EM noise

In transient electromagnetic instruments, several techniques are applied to suppress the EM noise. Firstly, the decay signal is integrated in gates having exponentially increasing width as a function of decay time (log-gating). The integration serves two major functions: (i) it reduces the dynamic range of the input signal and (ii) it reduces the bandwidth, as an integrator is inherently an LP filter with a frequency response of a sinc-function. Secondly, a synchronous detection technique (gate-stacking) is used in which the polarity of the transmitter wave is alternated between half-cycles. Synchronous detection removes the offset in the receiver amplifiers and makes it possible to use repetition frequencies of f/N, reducing power-line noise and increasing the S/N ratio at later times. f is the 50/60 Hz power-line frequency and N is an even number.

In order to reduce high-amplitude AM transmitter noise, most transient electromagnetic instruments are segmented such that each segment is band-limited by LP filters. The instrumentation is designed so that the bandwidth is broad at early time segments and narrow at late time segments. However, application of LP filters distorts the TEM response due to damping of the high-frequency content, as the cut-off frequency must be low enough to obtain a satisfactory S/N ratio.

In order to characterize the EM noise, two data sets were measured with a prototype TEM instrument (Sørensen 1997). The data sets were collected with a 10 kHz and a 500 kHz LP filter, respectively. The noise measurements were log-gated and gate-stacked (10 000 time series), and the mean and the standard deviations were calculated (Fig. 1). Figure 1a shows that the mean of the 500 kHz noise is about an order of magnitude higher at early times compared with the mean of the 10 kHz noise. The standard deviation falls off as t^{-1} for the 500 kHz noise, whereas the 10 kHz noise contains two time dependences. At times earlier than 10^{-3} s, the standard deviation exhibits a t^{-1} time dependence, whereas a $t^{-1/2}$ time dependence is seen for times later than 10^{-3} s.

In our experience the standard deviation, as in the case of the broadband (500 kHz) measurement in Fig. 1a, always exhibits a t^{-1} time dependence when the bandwidth is 100 kHz or higher. These observations indicate that the EM noise spectrum is coloured because a white noise spectrum, as shown by Munkholm and Auken (1996), is expected to show a $t^{-1/2}$ dependence when log-gated. Munkholm and Auken (1996) showed that several spectral peaks are present in the EM noise spectrum, indicating that the EM noise spectrum is coloured, and they recognized these as VLF and LF radio transmitters.

In order to test the above-mentioned observations, a numerical simulation of a log-gated and gate-stacked TEM receiver system was made. In the simulation two cases of noise spectra were considered: (i) a white noise spectrum and (ii) a noise spectrum containing a simulated AM transmitter in an otherwise white noise spectrum (AM noise spectrum). Figures 1c and d show three simulations: (i) a white noise spectrum, (ii) an AM noise spectrum and (iii) an AM noise spectrum band-limited with a 10 kHz

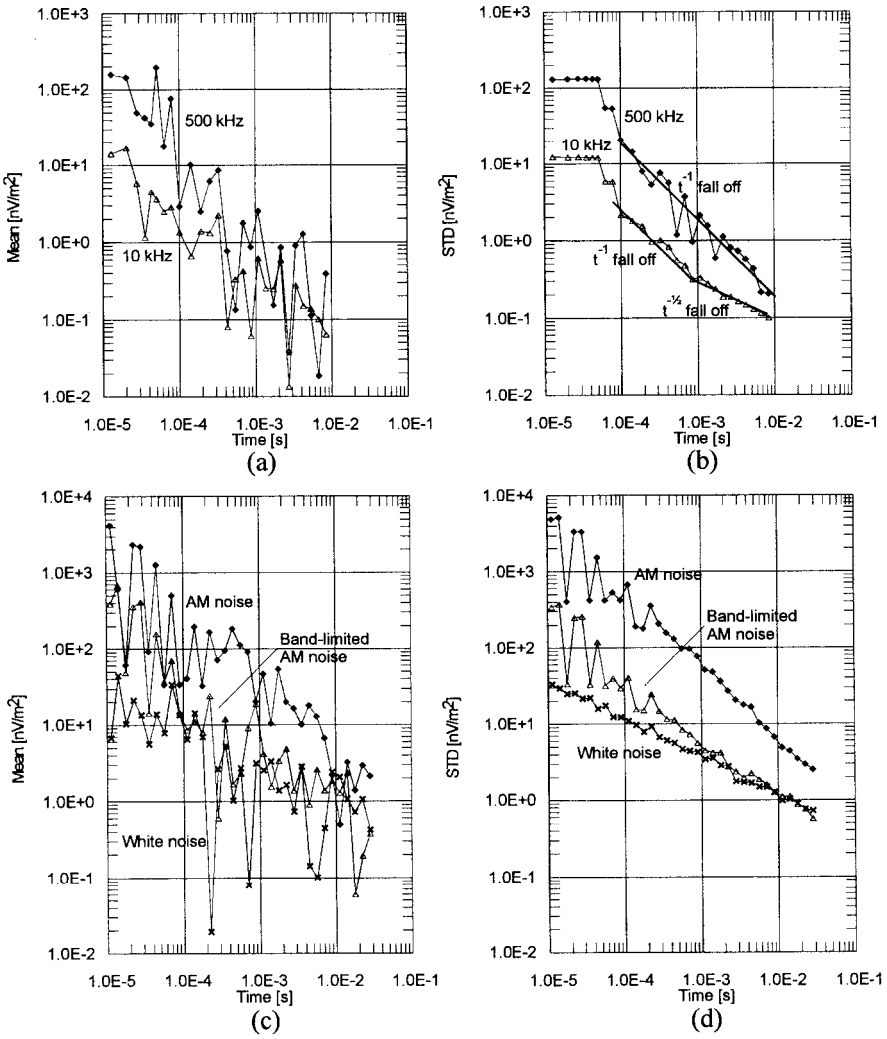

Figure 1. (a) and (b) Mean and standard deviation, respectively, of real noise data measured with a 10 and a 500 kHz LP filter. The mean of the 500 kHz data is significantly higher, about an order of magnitude at early times, than the mean of the 10 kHz data. For the 10 kHz data the standard deviation has a t^{-1} time dependence at early times, and a $t^{-1/2}$ time dependence at late times. The 500 kHz noise data has a t^{-1} dependence in the entire time range. (c) and (d) Numerical simulations of two noise spectra subjected to log-gating and gate-stacking. (c) and (d) show the mean and the standard deviations, respectively. One curve represents a white noise spectrum, the second curve represents a white noise spectrum superimposed with excess white noise in the frequency range 239–249 kHz (AM noise spectrum), and the third curve is the AM noise spectrum band-limited with a 10 kHz LP filter (thick curve).

LP filter. The AM transmitter was simulated by multiplying a white noise spectrum by a factor of 100 in the frequency range 239–249 kHz. This frequency range was chosen to simulate the high-amplitude LF radio transmitter present in Denmark. Log-gating was performed by equidistantly sampling and averaging over the samples within the time range of the gate. The mean and the standard deviation were calculated for 100 realizations of noise spectra, shown in Figs 1c and d, respectively.

Figure 1c shows that the mean of the AM noise is $\approx$5–10 times higher than the mean of the band-limited noise, up to about 10^{-2} s. Figure 1d shows that the standard deviation of the AM noise exhibits a t^{-1} time dependence, whereas the band-limited AM noise exhibits a t^{-1} dependence at early times and a $t^{-1/2}$ dependence at late times.

In conclusion the standard deviation of the broadband measurement (500 kHz) of the real noise and the broadband simulation of the AM noise spectrum indicate that the real EM noise spectrum is coloured as it shows a t^{-1} fall-off. The simulation, as well as observation of the EM spectrum, suggests that the t^{-1} fall-off (as opposed to a $t^{-1/2}$ fall-off for white noise) is probably due to the AM transmitters. The means of the real and the simulated noise indicate that band-limitation of the noise spectrum significantly reduces the noise amplitude. Accordingly, band-limitation of TEM responses will improve the S/N ratio and thereby enhance the depth of exploration of TEM soundings.

The inversion approach

We have implemented a numerical code for forward and inverse modelling of one-dimensional TEM data. The forward code includes modelling of LP filters and any piece-wise linear transmitter waveform (Raiche 1984; Asten 1987; Fitterman and Anderson 1987). The frequency- to time-domain transform is implemented as a straightforward Fourier transform (Anderson 1982; Newman, Hohmann and Anderson 1986). Even though this approach is slightly more computationally intensive, it has, in our experience, some advantages over the commonly used Gaver–Stehfest inverse Laplace transform method (Knight and Raiche 1982). The Gaver–Stehfest algorithm may show instability, and it provides an accuracy of no better than four digits. If LP filters are applied in the Laplace domain, inaccurate responses result due to instability of the inverse Laplace filter even when implemented in double precision.

The implementation of the inverse Fourier transform approach follows that of Newman *et al.* (1986). The real and the imaginary parts of the frequency-domain response represent the spectrum of a causal function, suggesting that the transformation from the frequency domain to the time domain is obtained by means of either a cosine or a sine transform. The step response is obtained from

$$f(t, p) = -\frac{2}{\pi}\int_0^\infty \frac{\mathrm{Im}[F(\omega, p)]}{\omega}\cos(\omega t)\,\mathrm{d}\omega \qquad (1)$$

or

$$f(t, p) = -\frac{2}{\pi}\int_0^\infty \frac{\mathrm{Re}[F(\omega, p)]}{\omega}\sin(\omega t)\,\mathrm{d}\omega, \tag{2}$$

and the impulse response from

$$\frac{\mathrm{d}f(t, p)}{\mathrm{d}t} = \frac{2}{\pi}\int_0^\infty \mathrm{Im}[F(\omega, p)]\sin(\omega t)\,\mathrm{d}\omega \tag{3}$$

or

$$\frac{\mathrm{d}f(t, p)}{\mathrm{d}t} = -\frac{2}{\pi}\int_0^\infty \mathrm{Re}[F(\omega, p)]\cos(\omega t)\,\mathrm{d}\omega, \tag{4}$$

where p is the model vector and $F(\omega, t)$ is the frequency-domain kernel. Johansen and Sørensen (1979) showed that the cosine and the sine transforms can be stated as $\mathrm{J}_{-1/2}$ and $\mathrm{J}_{1/2}$ transforms, respectively, so that

$$2\int_0^\infty F(x)^{\cos}_{\sin}(2\pi sx)\,\mathrm{d}x = r^{1/2}\int_0^\infty f_1(\lambda)\lambda \mathrm{J}_{\mp 1/2}(\lambda r)\,\mathrm{d}\lambda, \tag{5}$$

where $r = s(2\pi)^{1/2}$, $\lambda = x(2\pi)^{1/2}$ and $f_1(\lambda) = f(\lambda/(2\pi)^{1/2})\lambda^{1/2}$.

The integral in (5) is evaluated using the fast digital Hankel filters computed by Christensen (1990). The Hankel filters consist of precalculated filter coefficients, and the calculation is conducted as a discrete convolution between the filter coefficients and the frequency-domain kernels.

The TEM inversion is carried out as an iterative damped least-squares approach (Menke 1989), formally writing

$$\mathbf{m}_{n+1} = \mathbf{m}_n + (\mathbf{G}_n^{\mathrm{T}}\mathbf{C}_{\mathrm{d}}^{-1}\mathbf{G}_n + \alpha\mathbf{I})^{-1}\mathbf{G}_n^{\mathrm{T}}\mathbf{C}_{\mathrm{d}}^{-1}(\mathbf{d}_{\mathrm{obs}} - \mathbf{d}_n), \tag{6}$$

where $\mathbf{m}$ denotes the model vector, $\mathbf{G}_n$ is the Jacobian matrix, $\mathbf{C}_{\mathrm{d}}$ is the data covariance matrix, α is the damping factor, $\mathbf{I}$ is the identity matrix, $\mathbf{d}_{\mathrm{obs}}$ denotes the observed data vector and $\mathbf{d}_n$ denotes the forward data vector based on the previous model vector $\mathbf{m}_n$.

The model parameter analysis is based on the linear approximation to the covariance of the estimation error, $\mathbf{C}_{\mathrm{est}}$ (Jackson 1979; Menke 1989),

$$\mathbf{C}_{\mathrm{est}} = (\mathbf{G}^{\mathrm{T}}\mathbf{C}_{\mathrm{d}}^{-1}\mathbf{G})^{-1}, \tag{7}$$

where $\mathbf{G}$ is based on the final model obtained in the inversion.

The data fit is determined by the data residual, *RES*, given by

$$RES = \frac{1}{N}\sqrt{\sum_{n=1}^{N}\frac{(y_n - d_n)^2}{\sigma_n^2}}, \tag{8}$$

where d_n denotes the observed data, y_n denotes the predicted data, σ_n denotes the relative standard deviation and N is the number of data points.

Band-limitation of TEM responses

Band-limitation of TEM responses introduces errors due to damping of the high-frequency content. These errors depend on the cut-off frequency, transmitter waveform and subsurface resistivities. Hence TEM instruments are traditionally designed with a system bandwidth varying with the time segment. In early time segments the system has a broad bandwidth, which is gradually narrowed with increasingly later time segments. In this paper the effect of analog electronic filters is modelled by digital, first-order Butterworth filters. The filtered response is obtained by imposing the multiplication theorem on (1), formally writing

$$f(t, p) = -\frac{2}{\pi}\int_0^\infty \frac{\mathrm{Im}[F(\omega, p)H(\omega)]}{\omega}\cos(\omega t)\,\mathrm{d}\omega, \tag{9}$$

where $H(\omega)$ is the frequency response of the digital filter. For instance, a first-order LP Butterworth filter is given by

$$H_1(\omega) = \frac{1}{1 + \mathrm{i}\omega/\omega_c} \tag{10}$$

where ω_c is the cut-off frequency.

Distortion of TEM responses

In order to quantify the distortion of the TEM responses due to band-limitation, a filter index, *FI*, is used, given by

$$FI = \frac{f_n(t) - f_f(t)}{f_n(t)}, \tag{11}$$

where f_n and f_f are the unfiltered and filtered responses, respectively. *FI* is used to assess the relative difference between the filtered and unfiltered responses for a given resistivity model.

Figure 2a shows theoretical, LP-filtered, TEM responses generated for a three-layer model (model A, Fig. 2c). This model consists of a 10 Ωm layer of infinite thickness, overlain by a 100 Ωm (100 m thick) layer, overlain by an upper 30 Ωm (30 m thick) layer. Geologically, this model corresponds to a basement of highly conductive clays overlain by a coarse-grained sand/gravel overlain by a clay till. In addition to the unfiltered response, the data include band-limited responses in the range from 50 to 400 kHz. As expected, the distortion becomes larger and more prolonged as the cut-off frequency decreases. Figure 2b shows the filter indices, *FI*, of the filtered responses in Fig. 2a. If the first three microseconds are neglected, where some of the curves have sign shifts, we see that *FI* becomes higher at lower cut-off frequencies, as suggested by Fig. 2a. Moreover, it is seen that an increase of the cut-off frequency by a factor of two increases *FI* by a factor of two at late times.

Figure 2d shows theoretical, LP-filtered, TEM responses generated for a three-layer model (model B, Fig. 2f). This model consists of a 10 Ωm layer of infinite thickness,

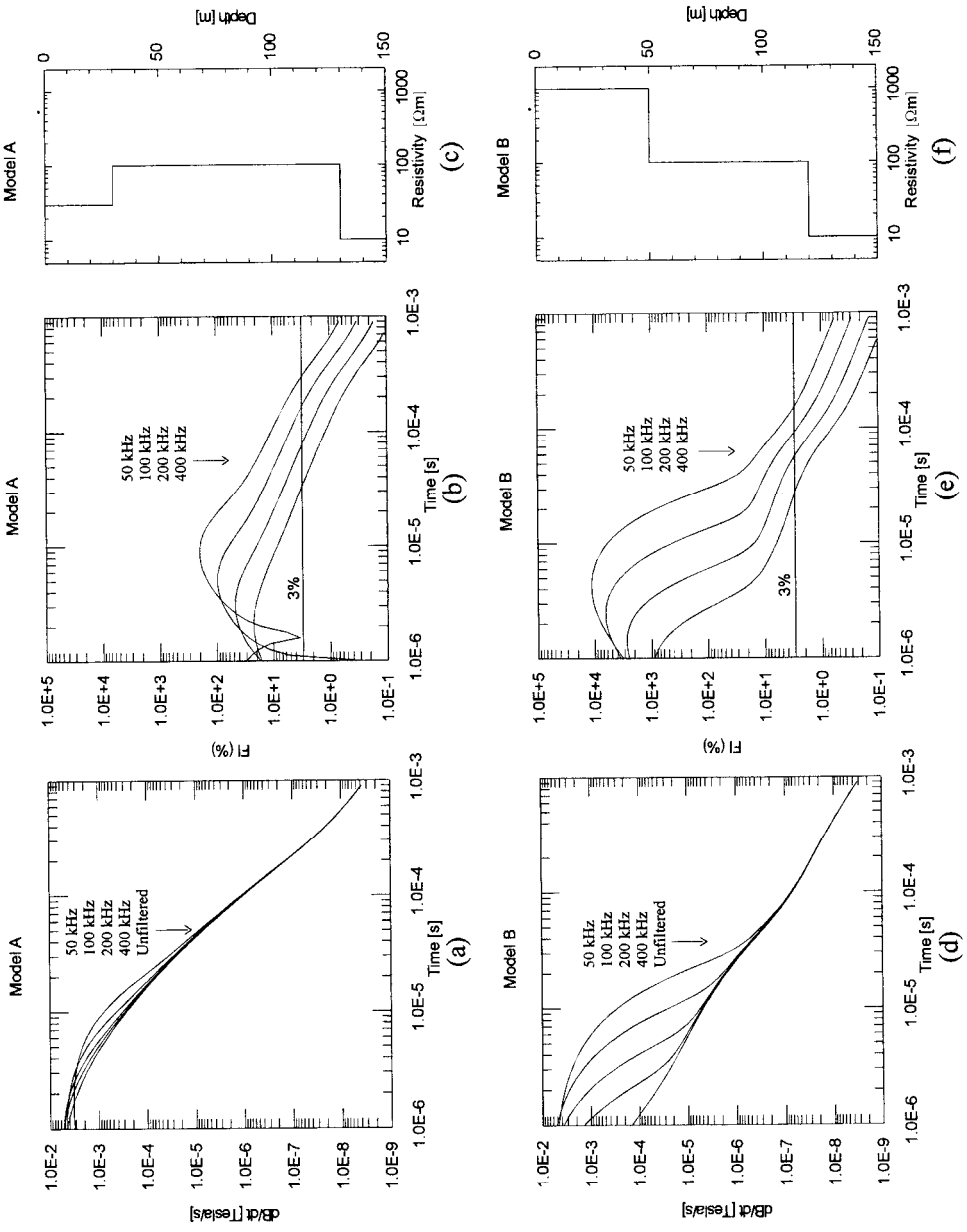
Model A
Model B
Depth [m]
Resistivity [Ωm]
(c)
(f)
50 kHz
100 kHz
200 kHz
400 kHz
Unfiltered
3%
FI (%)
Time [s]
(b)
(e)
dB/dt [Tesla/s]
(a)
(d)

overlain by a 100 Ωm (70 m thick) layer, overlain by an upper 1000 Ωm (50 m thick) layer. This model is similar to model A except that the upper layer consists of a thick unsaturated zone of sand instead of till. Figure 2e shows the *FI* for the responses in Fig. 2d. We find the same tendency for this model, namely that the distortion increases with decreasing cut-off frequency. Comparing the *FI* for models A and B, it is seen that the distortions of the responses for model B are significantly higher (about a factor of 100), but approach those for model A at late times.

Inversion of theoretical data

In order to test the effect of modelling the LP filters in the inversion scheme, theoretical response data were generated for models A and B. The responses consist of an early time (6 μs to 1 ms) segment and a late time (0.1 ms to 8 ms) segment. A 200 kHz and a 450 kHz LP filter and a 40 kHz and a 450 kHz LP filter were applied to the early time and late time segments, respectively. The 40 and the 200 kHz cut-off frequencies simulate the bandwidth of the receiver system, whereas the 450 kHz cut-off frequency simulates the bandwidth of the receiver coil. These cut-off frequencies were chosen as they are typical of those applied in commercial TEM instruments.

The theoretical data were modelled in two ways: one in which the LP filters were included in the inversion scheme, and one in which the filters were excluded from the inversion. The inversion results for model A are shown in Fig. 3, and the inversion results for model B appear in Fig. 4.

Figure 3c shows that a good model recovery and data fit with a residual of 0.84 is obtained when the LP filters are included in the inversion scheme. The parameter analysis shows that all model parameters are well determined with uncertainties less than 10%. In the case where the filters were excluded in the inversion, the data were modelled by a three- and a four-layer model (Figs 3d and e). The three-layer model results in a poor data fit, whereas the four-layer model produced a satisfactory data fit with a residual of 1.13. However, neither the three-layer model nor the four-layer model resulted in a good recovery of the original model. Of the model parameters in the three-layer model, only the third-layer resistivity resembles that of the initial model. The parameter analysis suggests, however, that all the model parameters are well determined. The four-layer model suffers from a false low resistivity: a top layer that does not resemble the top layer in the initial model. If the first layer is neglected the remainder of the model is very much like the initial model. The analysis shows that the top-layer parameters are completely undetermined and the other model parameters are

Figure 2. (a) Theoretical responses generated for model A in (c). The responses include an unfiltered response in addition to four responses filtered with, respectively, 50, 100, 200 and 400 kHz first-order LP filters. (b) Filter index (*FI*) for the responses in (a). (d) Theoretical responses for model B in (f). The LP filters are the same as in Fig. 3a. (e) *FI* for the responses in (d). The 3% line shown in (b) and (e) indicates the assumed noise level in the data.

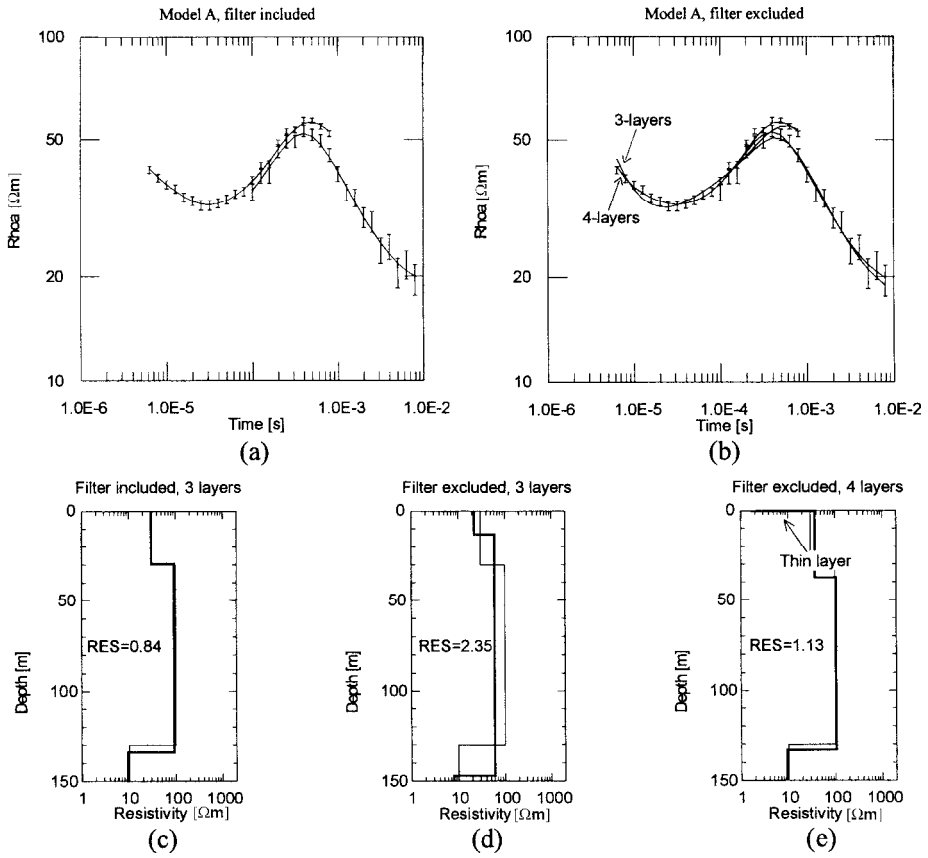

Figure 3. Theoretical data (error bars) in (a) and (b) generated for model A are shown as thin curves in (c)–(e). The theoretical data were generated using a 200 and a 450 kHz LP filter in the early time segment, and a 40 and a 450 kHz filter in the late time segment. 3% and 5% white noise was added to the early and the late time segments, respectively. The theoretical data were inverted with and without the LP filters included in the inversion scheme. The model response based on inclusion of the LP filters and the inverted model are shown in (a) (curve) and (c) (thick), respectively. In the inversion scheme without inclusion of the LP filters, the data were interpreted by (d) a three-layer model and (e) a four-layer model. Model responses for the three-layer (thin curve) and the four-layer (thick curve) models are shown in (e).

slightly less well determined compared with the inversion with the filter included. Thus, in this case it is necessary to add a false layer to the initial model when the filters are not included in the inversion scheme.

For model B (Fig. 4), the inversion with LP filters produces a good model recovery and data fit. In the inversion with LP filters excluded, the data were modelled with two three-layer models, namely one with all the data points and the other with the two data points (6–10 μs) removed. For the inversion with all data (no filters), a poor model recovery is obtained with a residual of 4.8. In the modelling where the first two data

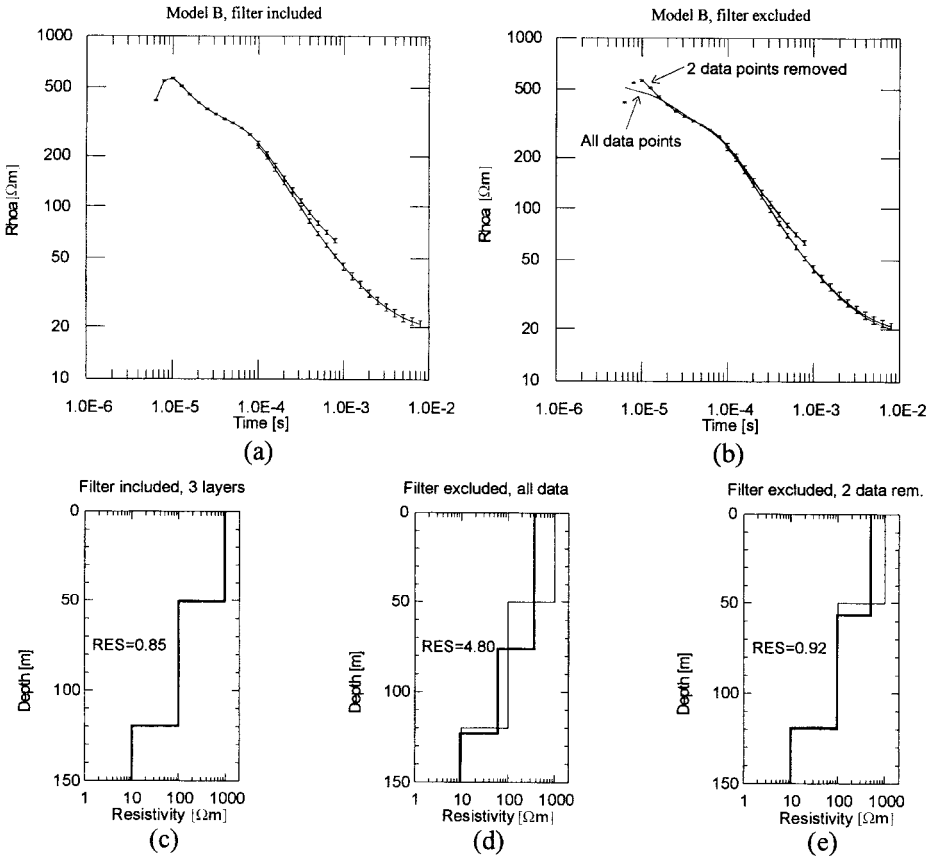

Figure 4. Similar annotations as in Fig. 3 apply to Fig. 4 where the theoretical data were generated for model B shown as thin curves in (c)–(e). In the inversion scheme without the inclusion of the LP filters, the theoretical data were inverted (d) using the full data set and (e) with the first two data points removed.

points were removed, the initial model is significantly better recovered with a residual of 0.92. All model parameters are determined better than 10%.

In conclusion, the effect of the LP filters is more pronounced at early times in the high-resistivity model (model B) compared with the low-resistivity model (model A). For the high-resistivity model, a reasonable model recovery is obtained by removing the first data points, whereas for the low-resistivity model the effect is more smeared out and it is not possible to recover the model by removing the early data points.

Inversion of field data

The inversion approach was applied to field data acquired at different cut-off frequencies. The geological model of the field site is considered to be a 40 m thick till on top of Tertiary

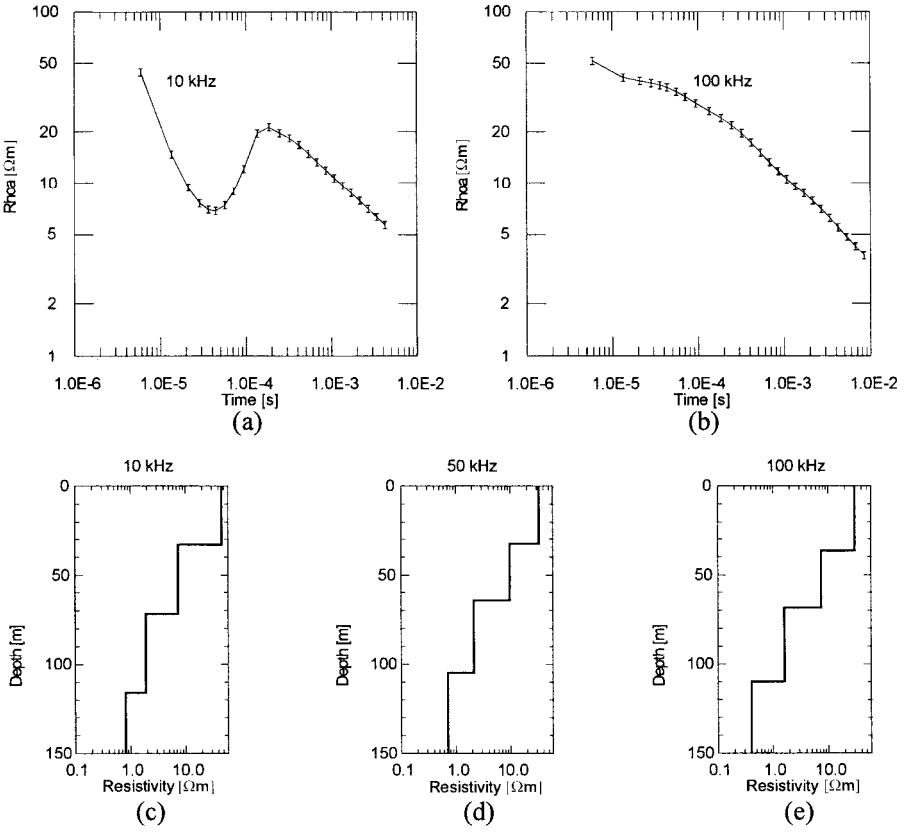

Figure 5. Field data (error bars) measured with (a) a 10 kHz first-order LP filter and (b) a 100 kHz first-order LP filter together with four-layer model responses (curve). (c)–(e) Inverted models obtained from field data collected with the 10, 50 and 100 kHz LP filters. Identical LP filters used to collect the data were included in the inversion scheme.

low-resistivity clays. Data were measured with a prototype TEM system. A receiver coil with a bandwidth of 1 MHz and an effective receiver area of 60 m^2 was used. The data were acquired in the central loop configuration using a square of 40 m × 40 m transmitter loop and a transmitter current of 7.6 A. Three different first-order LP filters with cut-off frequencies of 10, 50 and 100 kHz were used to collect separate data sets.

The data sets were modelled using LP filters with the same cut-off frequencies as were applied in measuring the data. In Figs 5a and b, the inversion results are shown for the 10 and 100 kHz data, and the inversion results for all the cut-off frequencies are shown in Figs 5c–e. As can be seen, it is possible to recover the same four-layer model within the uncertainties of the model parameters for all three data sets. However, the model parameter analysis shows that application of very low cut-off frequencies (10 kHz) may increase the parameter uncertainty of the uppermost layers due to the lack of the high frequencies.

Conclusions

Measured noise and simulation of the EM noise spectrum indicates that high-power amplitude-modulated VLF and LF radio transmitters are significant contributors to the overall noise level. The standard deviation of log-gated real noise exhibits a characteristic t^{-1} time dependence, being indicative of a coloured noise spectrum. Measurements of the real noise spectrum and simulated noise spectra show that band-limitation dampens the noise amplitudes significantly and thereby the influence of the AM transmitters. The noise reduction improves the S/N ratio and therefore the depth of exploration in TEM soundings.

Due to the AM transmitters it is mandatory to band-limit TEM responses to obtain a satisfactory depth of exploration. However, band-limitation will distort the TEM responses because of the damping of the high-frequency content. The distortion is dependent on several factors such as cut-off frequency and subsurface resistivities. The distortion increases at lower cut-off frequencies and higher resistivities.

It is demonstrated that distortions due to cut-off frequencies applied in commercial TEM instruments can lead to incorrect inversion results if the low-pass filters are not included in the inversion scheme. We have shown that for both theoretical and field data the applied low-pass filters can be incorporated in the inversion scheme. The inversion results obtained this way demonstrate that similar resistivity models within the uncertainties of the model parameters can be recovered, independent of the applied cut-off frequency.

References

Anderson W.L. 1982. *Nonlinear least-squares inversion of transient soundings for a central loop system (Subprogram NLSTCI).* US Geological Survey Open-File Report 82-1129, 85.

Asten M.W. 1987. Full transmitter waveform transient electromagnetic modeling and inversion for soundings over coal measures. *Geophysics* 52, 279–288.

Auken E., Christensen N.B., Sørensen K.I. and Effersø F. 1994. Large scale hydrogeological investigation in the Beder area – a case study. Symposium on the Application of Geophysics to Engineering and Environmental Problems (SAGEEP), Boston, USA, Expanded Abstracts, 615–628.

Christensen N.B. 1990. Optimized fast Hankel transform filters. *Geophysical Prospecting* 38, 545–568.

Christensen N.B. and Sørensen K.I. 1994. Integrated use of electromagnetic methods for hydrogeological investigations. Symposium on the Application of Geophysics to Engineering and Environmental Problems (SAGEEP), Boston, USA, Expanded Abstracts, 163–176.

Fitterman D.V. and Anderson W.L. 1987. Effect of transmitter turn-off time on transient soundings. *Geoexploration* 24, 131–146.

Jackson D.D. 1979. The use of a priori data to resolve non-uniqueness in linear inversion. *Geophysical Journal of the Royal Astronomical Society* 57, 137–157.

Johansen H.K. and Sørensen K. 1979. Fast Hankel transforms. *Geophysical Prospecting* 27, 876–901.

Knight J.H. and Raiche A.P. 1982. Transient electromagnetic calculations using the Gaver–Stehfest inverse Laplace transform method. *Geophysics* **47**, 47–50.

Macnae J.C., Lamontagne Y. and West G.F. 1984. Noise processing techniques for time-domain EM systems. *Geophysics* **49**, 934–948.

McCracken K.G., Oristaglio M.L. and Hohmann G.W. 1986. Minimization of noise in electromagnetic exploration systems. *Geophysics* **51**, 819–832.

Menke W. 1989. *Geophysical Data Analysis: Discrete Inverse Theory.* Revised edn. Academic Press Inc.

Munkholm M.S. and Auken E. 1996. Electromagnetic noise contamination on transient electromagnetic soundings in culturally disturbed environments. *Journal of Environmental and Engineering Geophysics* **1**, 119–127.

Newman G.A., Hohmann G.W. and Anderson W.L. 1986. Transient electromagnetic response of a three-dimensional body in a layered earth. *Geophysics* **51**, 1608–1627.

Raiche A.P. 1984. The effect of ramp function turn-off on the TEM response of layered earth. *Exploration Geophysics* **15**, 37–41.

Sørensen K.I. 1996. Detailed regional hydrogeophysical investigations – the Solbjerg case. Symposium on the Application of Geophysics to Engineering and Environmental Problems (SAGEEP), Keystone, USA, Expanded Abstracts, 343–352.

Sørensen K.I. 1997. The pulled array transient electromagnetic method. *Proceedings of the 3rd EEGS Meeting, Aarhus, Denmark*, pp. 135–138.

Spies B.R. and Frischknecht F.C. 1991. Electromagnetic sounding. In: *Electromagnetic Methods in Applied Geophysics* (ed. M.N. Nabighian), pp. 285–425. Society of Exploration Geophysicists.